Model study of keV-ion mixing of metallic interfaces: Influence of materials properties and deposited energy

Heinrich Gades and Herbert M. Urbassek
Fachbereich Physik, Universität Kaiserslautern, Erwin-Schrödinger-Straße, D-67663 Kaiserslautern, Germany
(Received 3 January 1995)

Using molecular-dynamics simulation, we study the mixing induced by keV ions in metals and metallic bilayers and its dependence on materials properties. This is possible since we use many-body potentials of the tight-binding form, in which the cohesive energy and the heat of mixing can be independently assigned. In the simulations, the interface mixing shows an inverse-square dependence on the cohesive energy, and a stronger than linear dependence on the heat of mixing. Both features are in accordance with the experimental observations, and with existing phenomenological models. Mixing depends quadratically on the deposited energy. These features are in even quantitative agreement with a phenomenological model of thermal spike mixing. Only small mass effects in the mixing of isotopic systems are observed.

I. INTRODUCTION

When an interface is bombarded by energetic ions, atoms may be displaced from each side of the interface into the other, and hence the material is mixed.[1,2] This ion-beam-induced mixing effect has been used to create metastable phases of materials.[3] On the other side, it may be detrimental, for instance in the application of the sputter depth profiling technique for surface analysis.[4] Various mechanisms have been formulated to govern the mixing process.[1–5] First, the knock-on relocation of atoms from their lattice sites by the ion or other cascade atoms will contribute (collisional mixing). Second, at higher temperatures—which may also be existing in the thermal spike created by the ion bombardment—diffusion processes may be enhanced, either due to the surplus of point defects created or due to a transient melting of the spike region. Finally, chemical forces may bias the fluxes; this may happen either in the collisional phase (chemically guided motion)[6] or in a thermal spike.[5,7] From a theoretical point of view, collisional mixing has been studied both analytically[8–10] and by computer simulation[11] to a considerable degree. In contrast, thermodynamic and chemical forces have mostly been incorporated in the understanding of mixing by phenomenological models.[5–7,12–14] Molecular-dynamics simulations have been performed, but mostly with the aim of defining and understanding the concept and the role of the thermal spike.[15,16]

In the present paper, we shall use systematic molecular-dynamics simulations in order to study the effect of the materials parameters (chemical forces) on the mixing behavior. To this end, we shall investigate the mixing of pure Cu and of various model metals. The many-body potential of Cu, which we use, will allow us to modify independently the cohesive energy of this material, and the heat of mixing of a metal pair. This will allow us to study quantitatively the influence of these two material parameters on the mixing process. We shall see that the results obtained will compare favorably with the experiments, and with phenomenological models. We note that the present study concentrates on producing statistically reliable data on average quantities, which may be used for checking against phenomenological models. We did not analyze the data on a single-event atomistic scale, and will hence not immediately provide a microscopical picture of the mechanisms of mixing.

In molecular-dynamics computer simulation, we cannot perform systematic and statistically reliable studies with ion energies above a few keV. Hence, our studies are of most interest to keV mixing processes. For this reason, we investigate a near-surface geometry, where a surface film with a thickness of a few monolayers is mixed into the substrate. However, we believe that some of our results can also be used for an understanding of materials effects in high-energy mixing, in so far as local, low-keV subcascades are important for mixing. Of course, a number of effects present in high-energy cascades—such as recoil implantation, or spike (i.e., subcascade) overlap—are not covered by the present approach.

II. METHOD

We use a standard molecular-dynamics code.[17] Our simulation crystallite has a free unrelaxed (100) surface; the other five sides contain two layers of damped atoms in order to simulate the environment of the crystallite. It contains 11 435 atoms in 21 layers; its lateral extension is 33 ML. Because of damping, atom motion in the last two layers will not be recorded. The crystallite is kept at 0 K at the beginning of the simulation. The simulation is terminated at 8 ps after the projectile impact. Each simulation consists of a series of 25 events; in each event, a projectile hits a virgin crystallite with a random impact parameter in a symmetry-reduced unit cell in the middle of the crystal surface. The results shown are averages over these 25 events; error bars in the figures indicate the

mean error of the average values. In some simulations we shall use a bilayer crystal. In these cases, the first six near-surface monolayers will consist of a different material than the deeper layers.

The target atoms interact via a many-body potential of the tight-binding form.[18,19] For the pure Cu material, it is fitted to the cohesive energy E_{coh}, the lattice constant, the bulk modulus, and the vacancy formation energy. In all simulations performed in this paper, we keep the lattice-constant constant and equal to the experimental value of Cu (3.615 Å).[20] Furthermore, whenever we change the cohesive energy, we also change the bulk modulus and the vacancy formation energy by the same factor; thus, in our present paper, the value of the cohesive energy uniquely defines our (monatomic) material. Such a proportionality appears to be rather well fulfilled experimentally;[21] we also use it here in order to be able to employ the same cutoff radius (4.7 Å) for all materials without introducing too large a potential step.

When two different materials are used, the interspecies potential needs to be defined. In our many-body framework,[19] only two more parameters enter: the dilute heat of solving an atom A into the pure material B, ΔE_{AB}, and vice versa. We assume both to be equal. Usually, instead of the dilute heat of solution, the heat of mixing, ΔH_{mix}, is used to characterize the interspecies potential. In a regular solution, it is $\Delta H_{\mathrm{mix}} = c_A c_B \Delta E_{AB}$, where c_i is the atom concentration of species i in a homogeneous alloy, and $\Delta E_{AB} = \Delta E_{BA}$ holds rigorously. As for pair potential interaction, it can be shown for those of our many-body potentials, where the two metals agree in all their monatomic material parameters, that the same relationship holds; here, the so-called total-smearing model must be used. Hence, when presenting our mixing results for this class of alloys, we shall use $\Delta H_{\mathrm{mix}} = \Delta E_{AB}/4$.

We display in Fig. 1 a number of potentials, which will be used in the present investigation. Of the many ways which exist to display many-body potentials, we chose to present dimer potentials.

For high interaction energy, the potentials are fitted to the ZBL potential;[22] for this always the values for Cu are used. In order to have the same repulsive properties of the target particles in the collision cascade at high energies, care was taken that the fit only influenced the potential at energies below 9 eV, when E_{coh} was varied [Fig. 1(a)], and 45 eV, when ΔH_{mix} was varied [Fig. 1(b)]. We note that no electronically inelastic losses were taken into account in the simulation.

The projectile was always chosen as Cu, and interacts via the purely repulsive ZBL potential with the target atoms. It impinges in the normal direction with an energy of 1 keV; only in Secs. III E and III F the projectile energy and angle of incidence will be changed. We note that 1 atom impinging on the surface of our crystallite corresponds to a fluence of $\phi = 3.0 \times 10^{12}\ \mathrm{cm}^{-2}$.

III. RESULTS

A. Reference case

In the following, we shall discuss the mixing of a pure Cu target. This will serve both to introduce the quantities monitored, and as a reference case. We have tried to extract from our simulations the spatial extension of the collision cascades. To this end, we aimed at monitoring the deposited energy distribution. This quantity, however, is not immediately detectable in a molecular-dynamics

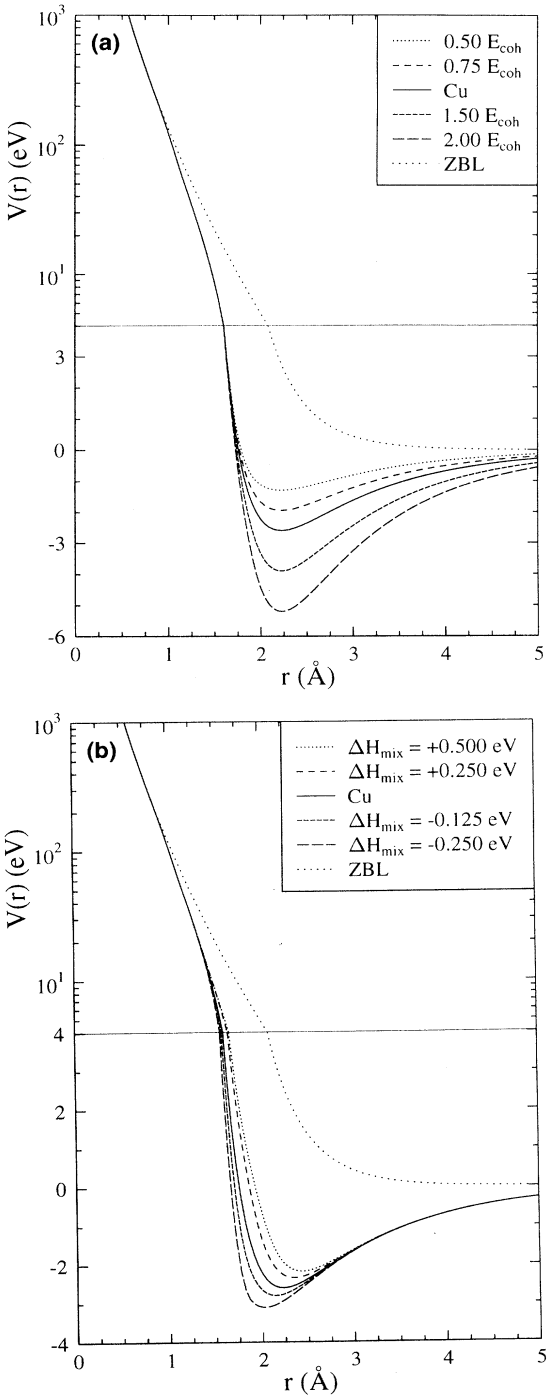

FIG. 1. Dimer potentials extracted from the many-body potentials used in this study (a) for two Cu atoms with decreased (increased) cohesive energy, (b) for two Cu atoms with positive (negative) heat of mixing. For comparison, the purely repulsive ZBL potential has been included.

simulation. We monitor two related quantities: The number $N_{\rm rec}(z,E_c)\Delta_z$ of recoils created in layer z (interlayer spacing Δz) with an energy above energy E_c, and the depth distribution of recoil energy, $E_{\rm rec}(z,E_c)$, which we define as the total amount of kinetic energy of the recoils created in layer z with minimum energy E_c. In the linear cascade regime, the number of recoils is proportional to the deposited energy,[23]

$$E^{(1)}_{\rm dep}(z,E_c)=\frac{E_c}{\Gamma_m}N_{\rm rec}(z,E_c)\Delta z \ . \tag{1}$$

We denote the deposited energy calculated from the number of recoils by $E^{(1)}_{\rm dep}$. The quantity Γ_m depends weakly on the interatomic potential; it is set equal to $\Gamma_m=0.52$.[24] The recoil energy $E_{\rm rec}$ is not identical to the deposited energy, on the one hand, since contributions of potential energy are not included in the monitoring of $E_{\rm rec}$, and on the other hand, since one recoil may give energy to another recoil in the same layer, and both are counted to contribute to $E_{\rm rec}$. We, therefore, calculate the deposited energy, $E^{(2)}_{\rm dep}$, by normalizing the deposited energy to the bombarding energy, E_0, and the layer-resolved recoil energy $E_{\rm rec}(z,E_c)$ to the total layer-integrated recoil energy, $E_{\rm rec,tot}(E_c)=\sum_z E_{\rm rec}(z,E_c)$:

$$\frac{E^{(2)}_{\rm dep}(z,E_c)}{E_0}=\frac{E_{\rm rec}(z,E_c)}{E_{\rm rec,tot}(E_c)} \ . \tag{2}$$

While the first definition is an obvious implementation of the linear cascade ideas, and will be valid at not too small cutoff energies E_c, larger than some tens of an eV, say, we use the second detection scheme for the deposited energy as a control of how sensitive this quantity is with respect to the detection mechanism. The methods described here become invalid as soon as a noticeable part of the incident energy is deposited outside the simulation crystallite; we checked that this is the case for bombarding energies above 2 keV.

We, furthermore, note that the notion of a deposited energy is not well defined in a molecular-dynamics simulation, where all energies are finally carried away by phonons. The difficulties of defining a recoil and its energy in a molecular-dynamics simulation have been discussed elsewhere.[24]

For further reference we define—quite arbitrarily—as the deposited energy in layer z the quantity,

$$F_D(z)=\frac{E^{(2)}_{\rm dep}(z,E_c=1\ {\rm eV})}{\Delta z} \ . \tag{3}$$

Figure 2 shows that the two definitions used to obtain an estimate of the deposited energy distribution coincide reasonably well. Furthermore, the effect of lowering the cutoff energy E_c is obvious, in that the distribution broadens out and becomes smoother, while energy is dissipated away into the depth of the crystal. The center of the cascade (maximum of the deposited energy) is situated at around the fourth monolayer, but tends to move inward with decreasing E_c. At the interface between the sixth and seventh monolayer, which will be of interest in our studies of bilayer interface mixing, the deposited energy amounts to roughly 75 eV per monolayer, i.e., $F_D(z=6.5)\cong 40$ eV/Å, if the $E^{(2)}_{\rm dep}$ data for $E_c=1$ eV are used. We note that the form of the deposited energy distribution does not vary when the details of the many-body attraction are changed in the series of systematic simulations displayed below. This is due to the fact that the shape is determined by the repulsive high-energy interactions, which have been modeled to be identical in all of the simulations presented in this paper.

A basic quantity extracted from the simulation is the average number of target particles relocated from atomic layer z to atomic layer $z+\zeta$, which will be denoted by $\Delta N(z\rightarrow z+\zeta)$. It is connected to the well-known relocation cross section $d\sigma(z\rightarrow z+\zeta)$ from analytical theory[8–10] by $\Delta N=n\,d\sigma\Delta z$, where n is the number den-

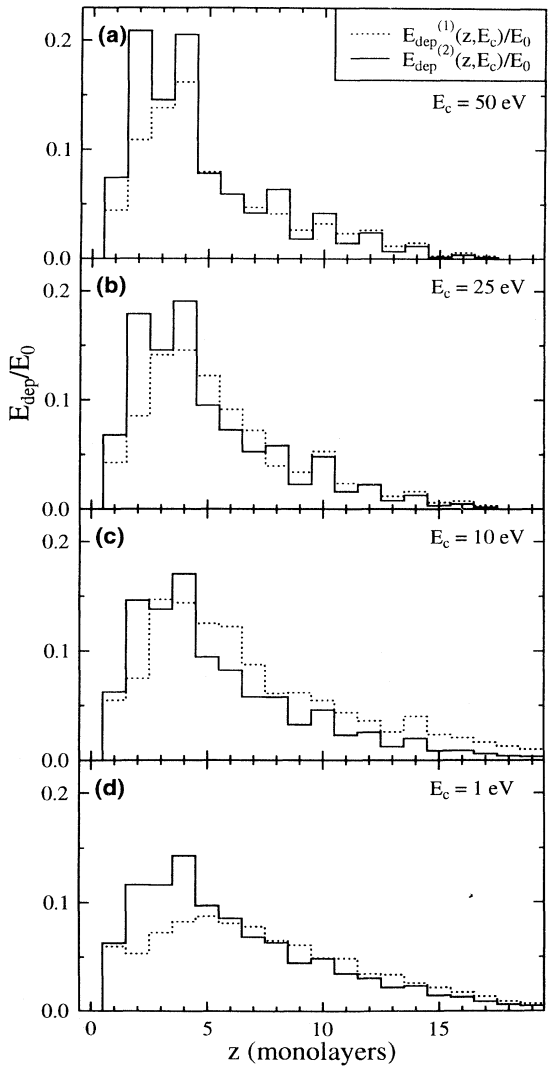

FIG. 2. Energy deposited per layer in a pure Cu sample, due to 1-keV Cu bombardment. Only recoils above cutoff energy E_c are taken into account. Two different detection schemes for the deposited energy are used, one based on the number of recoils created, $E^{(1)}_{\rm dep}$, cf. Eq. (1), and another one based on the maximum energy given to recoils, $E^{(2)}_{\rm dep}$, cf. Eq. (2).

sity of the target, and Δz is the interlayer spacing, i.e., half a lattice constant for our case of a (100) surface. This quantity contains a lot of detailed information on the mixing process. We plot in Fig. 3(a) two moments of this quantity, the shift s and the broadening b. The shift is defined as

$$s(z)=\int \zeta\, d\sigma(z\rightarrow z+\zeta)=\frac{1}{n\Delta z}\sum_{\zeta}\zeta\Delta N(z\rightarrow z+\zeta)\ . \quad (4)$$

$\phi s(z)$ hence gives us the average depth over which a target atom, which has initially been situated at depth z, is relocated due to an ion fluence ϕ. The broadening b is defined as

$$b(z)=\int \zeta^2 d\sigma(z\rightarrow z+\zeta)=\frac{1}{n\Delta z}\sum_{\zeta}\zeta^2\Delta N(z\rightarrow z+\zeta)\ . \quad (5)$$

$\phi b(z)$ describes the broadening of a marker layer initially situated at depth z and can be related to a diffusion coefficient D via $b\phi=2Dt$ where the time $t=\phi/I$ is the irradiation time (I is the ion flux). Evidently, b can also be used to characterize other kinds of mixing phenomena, such as the interface mixing in which we are interested here.

The broadening distribution [Fig. 3(a)] shows a monotonic decay into the target; it does not follow the near-surface depression of the deposited energy function. This is undoubtedly due to the presence of the surface, which facilitates particle motion there. This becomes clear from a comparison with Fig. 4 below: for diminished cohesive energy, the broadening distribution follows more directly the deposited energy function.

The shift presented in Fig. 3(a) is negative down to the ninth layer, i.e., directed towards the surface, and more or less vanishes deeper inside the target. The sign of the shift is astonishing. We interpret it to be due to the presence of the surface, which may influence particle motion down to large depths, since it constitutes a sink for all point defect motion. Thus, we think that the shift is of a mainly relaxational nature.

In order to get a more quantitative insight into the magnitude of the shift and the broadening, we plot the corresponding shift length ϕs and the broadening distance $\sqrt{\phi b}$ in Fig. 3(b) for our fluence of $\phi=3.0\times10^{12}$ cm^{-2}. We see that the broadening distance, i.e., the average distance in depth direction covered by a target atom during the bombardment fluence ϕ, is an order of magnitude larger than the shift, which represents the directional motion of target atoms. In the following, we shall hence concentrate on discussing the broadening distribution.

In Fig. 3(c), we compare the (vectorial) root-mean-square displacement $r^2(z)$ of particles, which start from layer z, with the component in depth direction, $r_\perp^2$. If the relocation is isotropic, we should expect $r_\perp^2=r^2/3$. As Fig. 3(c) shows, this is well fulfilled below the second monolayer. At the surface, $r^2/3>r_\perp^2$, since the lateral mobility is strongly enhanced at the surface, where adatoms are formed. Of course, $r_\perp^2$ is identical to ϕb, as displayed in Fig. 3(b). Small numerical deviations between these two quantities are due to the fact that when monitoring b, particle displacement was only measured in units of layer spacings, while we were more accurate in monitoring the quantities of Fig. 3(c); thus, small deviations may be due to the effect of thermal and defect-induced disorder in the end positions of the relocated atoms.

Sometimes an adjoint (or backwards) shift and broadening distribution can be of interest. These are defined as

$$\tilde{s}(z)=\int \zeta\, d\sigma(z-\zeta\rightarrow z)\ ,$$
$$\tilde{b}(z)=\int \zeta^2 d\sigma(z-\zeta\rightarrow z)\ , \quad (6)$$

and give information on how far a particle traveled until it reaches its final position in layer z. These quantities are displayed Fig. 3(d). The broadening resembles the forward broadening shown in Fig. 3(a). The shift is negative, i.e., directed towards the surface, at the near-surface side of the cascade; beyond the core of the cascade at layer 5, particles are displaced deeper into the target. When compared with the form of the deposited energy distribution, Fig. 2, it is seen that particle motion is predominantly away from the cascade core, i.e., into the target inner at larger depths and towards the surface at small depths. Its general form thus resembles the one found for Monte Carlo simulations of keV-ion-induced mixing.[25] The adjoint shift at layer 0 denotes the motion of atoms, which have come to rest at an adatom position. Note also that the adjoint shift at the layer 1 is more than a factor 2 larger than its forward quantity displayed in Fig. 3(a); this is due to the fact that atoms are more likely to end their motion in layer 1 than to start their motion there.

In Fig. 3(e), we show the net number of particles relocated from or to layer z. It is defined as

$$N_{\text{reloc}}(z)=\sum_{\zeta}[\Delta N(z-\zeta\rightarrow z)-\Delta N(z\rightarrow z+\zeta)]\ , \quad (7)$$

and is proportional to the relocation function of analytical theory.[26] In the case that different species are present in the target, it is connected with the concentration change in layer z. We note that with the possible exception of large depths, all layers are depleted from particles. The form of the depletion follows the deposited energy function in that it shows a local maximum around layer 5. The surface, however, has a strong effect: The first layer—and to a lesser degree also the second layer—is strongly depleted due to the formation of surface vacancies; on the other hand, adatoms are formed, which are indicated on layer 0 in the figure.

B. Effect of cohesive energy

We now examine the effect of an increased or decreased cohesive energy E_{coh} on the mixing behavior. At first we shall concentrate on the broadening in a monatomic material [Fig. 4(a)]. The quantitative effect of E_{coh} is large; recoil displacements are greatly facilitated by a decrease of the cohesive energy. Qualitatively, for large values of the cohesive energy, the broadening shows con-

siderable similarity with the deposited energy distribution. In this case, they both exhibit a maximum in the first few monolayers inside the target.

We also investigated the mixing in a bilayer system, in which the first six monolayers are formed of ordinary Cu, and the substrate below displays a modified cohesive energy [Fig. 4(b)]. The main effect appears to be that in a region extending several monolayers at each side of the interface, the mixing is determined by both materials. This is particularly clearly seen in the case where ordinary and weak Cu (i.e., Cu with a reduced cohesive energy) are mixed. There also on the Cu side considerably more mixing occurs than in the case of a pure Cu specimen.

We display in Fig. 5 the dependence of the broadening in layers 6 and 7 on the cohesive energy, both for the mixing in elemental metals and in bilayer systems. From the double-logarithmic presentation, a dependence $b \propto E_{\mathrm{coh}}^{-2}$ can be read off. We, furthermore, note that on closer inspection the mixing of elemental metals appears

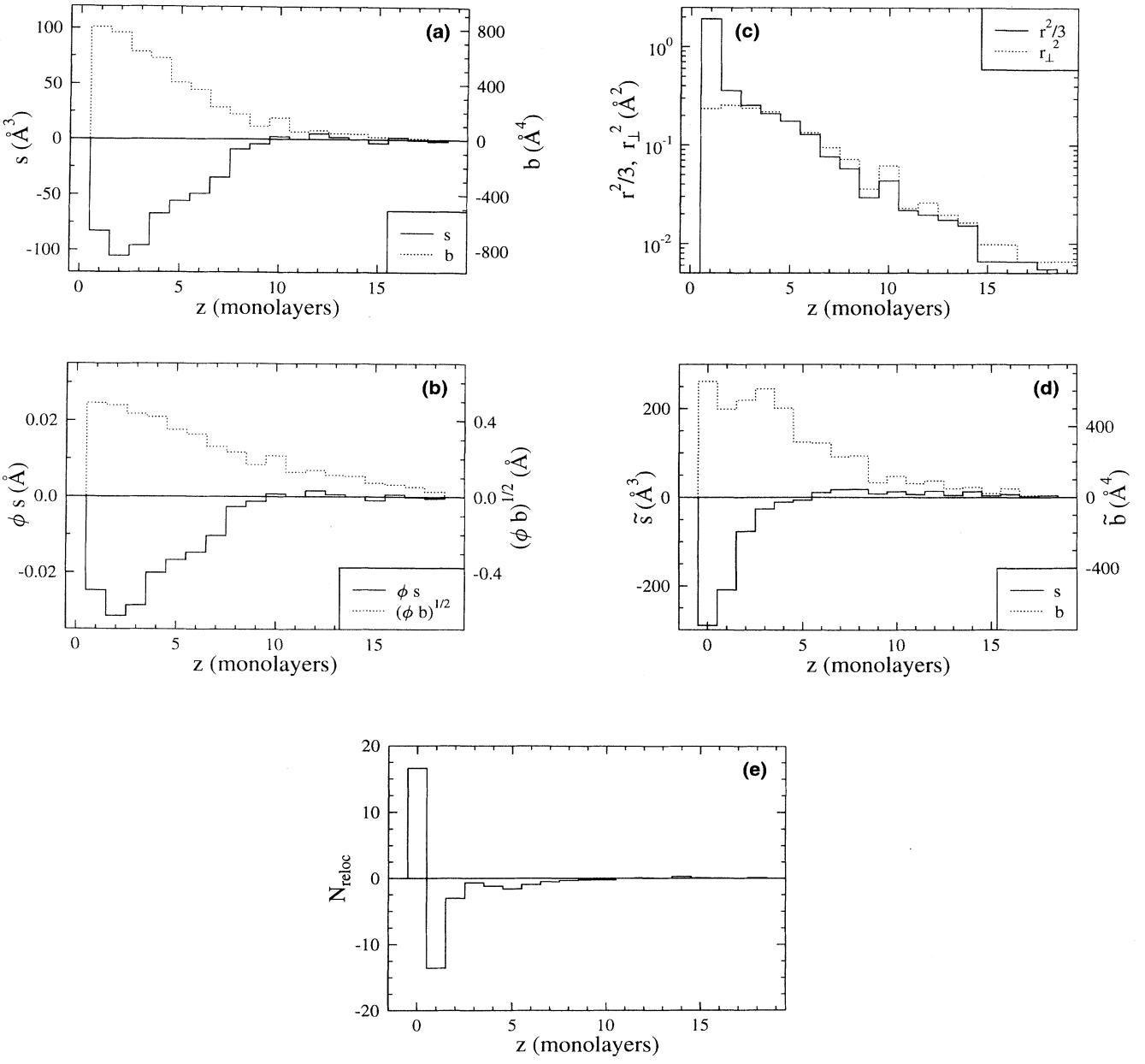

FIG. 3. Mixing in a pure Cu sample due to 1-keV Cu bombardment, corresponding to a fluence $\phi = 3 \times 10^{12}$ cm^{-2} as a function of the depth z inside the target. (a) Broadening b and shift s. (b) Displacement due to shift, ϕs, and broadening length $\sqrt{\phi b}$. (c) Mean-square vectorial displacement r^2 and its component in depth direction, $r_\perp^2$. (d) Adjoined broadening $\tilde{b}$ and shift $\tilde{s}$. (e) Net number of displaced atoms N_{reloc}.

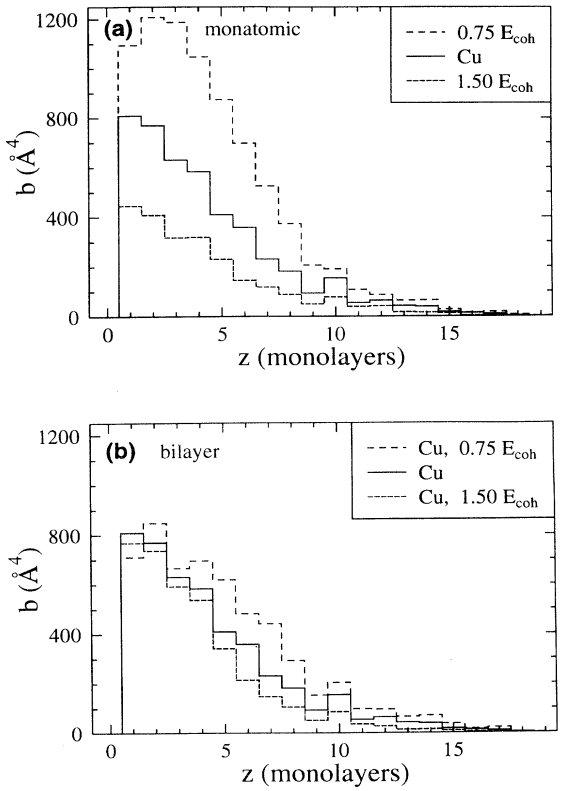

FIG. 4. Effect of cohesive energy E_{coh} on the broadening b in pure samples with altered cohesive energy (a), and for bilayers (b) in which the first six layers correspond to natural Cu, and the substrate to Cu with altered cohesive energy.

to show deviations from the E_{coh}^{-2} behavior; in particular, the system with the lowest cohesive energy shows a more drastic broadening than that expected from the quadratic dependence. We assume this behavior to result from the establishment of a particularly pronounced spike in this weakly bonded material.

In Fig. 5, we also compare the results of our simulations with the quantitative predictions of a phenomenological model, in which broadening is assumed to be due to the atom diffusion in a thermal spike.[5,7] In our notation, the model predicts the broadening as

$$b=\frac{k_1}{n^{5/3}}\left[\frac{F_D}{E_{\mathrm{coh}}}\right]^2\left[1-k_2\frac{\Delta H_{\mathrm{mix}}}{E_{\mathrm{coh}}}\right], \tag{8}$$

where the constants are given as $k_1=0.035$ Å, and $k_2=27.4$ from comparison of the model to experimental data.[5,7] We set the deposited energy at the interface, $F_D=F_D$ $(z=6.5)$, equal to our simulation result for $E_{\mathrm{dep}}^{(2)}$ for $E_c=1$ eV; as Fig. 5(d) shows, this quantity is rather independent of E_{coh}. Note that the authors of this formula usually give the left-hand side as $d(4Dt)/d\Phi$; however, they identify $4Dt$ with the variance of an initially sharp impurity profile. As the figure shows, Eq. (8) gives a satisfactory quantitative description of our simulation results. In particular, it also describes well the mixing of the pure Cu specimen.

In Figs. 5(b) and 5(c) the broadening in layers 6 and 7 in a bilayer material is displayed. While in Fig. 5(b) the broadening in these two layers is plotted separately as a function of the cohesive energy of this layer, in Fig. 5(c) the mean value of the broadening in these two layers is plotted as a function of the average cohesive energy of the two materials. As we see in Fig. 5(b), the broadening in the natural Cu layer strongly depends on the presence of an adjacent layer with changed cohesive energy; correspondingly, the mixing on the modified Cu side does not depend as strongly on its cohesive energy as in a monatomic material. As Fig. 5(c) shows, the average broadening depends even stronger than quadratically on the averaged cohesive energy.

Figure 6 shows the net particle fluxes through the bilayer interface, defined as the total number of atoms originating from layers 1 through 6 (top) and being displaced through the interface to layer 7 or below (below), or vice versa. In the case of a bilayer material, these fluxes directly give us the number of atoms displaced into a foreign material. Apart from the obvious feature that fluxes become stronger in weaker materials, the main trend appears to be that the weaker the material, the more atoms are displaced from deeper inside the material towards the near-surface layers. This might be correlated with the relaxational effect of the surface, which has been discussed above; in the case of a bilayer, it corresponds to the increased mobility of atoms in more weakly bonded solids. Note again the effect of the adjacent material on the particle fluxes [Figs. 6(b) and 6(c)], for which a representation by average quantities [Fig. 6(c)] displays a particularly strong effect.

C. Dependence on heat of mixing

For a precipitating system, i.e., $\Delta H_{\mathrm{mix}}>0$, only little differences to the reference case of pure Cu can be observed, cf. Fig. 7(a); yet the broadening is definitely smaller than in the reference case of vanishing mixing enthalpy, and the shift decreases pronouncedly between layers 6 and 7. However, for a system with negative heat of mixing, $\Delta H_{\mathrm{mix}}<0$, a considerable change of mixing at the interface is observed, Fig. 7(b). Not only the broadening increases there, but, in particular, the shift changes sign such as to enhance the particle fluxes crossing the interface. The effect of the heat of mixing on the broadening is summarized in Fig. 8. Note the small effect for small $|\Delta H_{\mathrm{mix}}|$ and the drastic increase of broadening for large negative ΔH_{mix}. This is a definitely nonlinear behavior. It is in agreement with the experiments, as has been noted previously.[5,13] The phenomenological model of Ref. 5, Eq. (8), approximates it by a linear law; this is bound to fail for large negative heats of mixing, and does not give justice to the nonlinear behavior seen here and in the experiment. We note that the behavior shown in Fig. 8 can be fitted by a law of the form

$$b=\frac{k_1}{n^{5/3}}\left[\frac{F_D}{E_{\mathrm{coh}}}\right]^2\left[1-h\left[\frac{\Delta H_{\mathrm{mix}}}{E_{\mathrm{coh}}}\right]\right], \tag{9}$$

where the linear term $h(\varepsilon)=k_2\varepsilon$ of Eq. (8) now reads

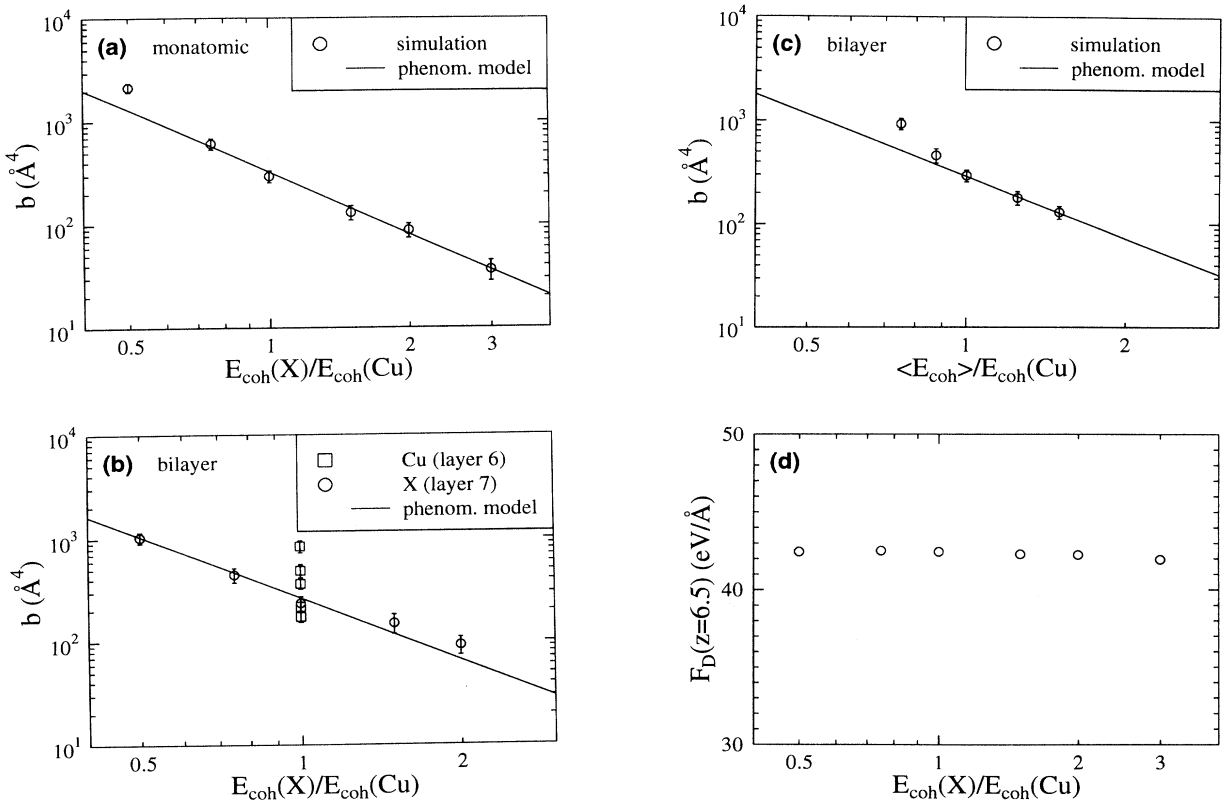

FIG. 5. Effect of cohesive energy on broadening in elemental samples (a) and in bilayers (b,c). The altered cohesive energy is denoted by $E_{coh}(X)$ and given in units of the cohesive energy of pure Cu, $E_{coh}(Cu)$. While in (b) the broadening of layers 6 and 7 are also plotted separately, only their mean value is shown in subfigures (a) and (c). The average cohesive energy is denoted by $\langle E_{coh} \rangle = [E_{coh}(Cu) + E_{coh}(X)]/2$. Lines represent the phenomenological model of Ref. 5, Eq. (8). (d) Dependence of deposited energy F_D ($z = 6.5$) on cohesive energy E_{coh} in elemental samples.

$$h(\varepsilon) = 0.24(1 - e^{-37\varepsilon}) . \quad (10)$$

This is to be taken as a fit formula without theoretical foundation. We do not understand the origin of the increased mixing for strongly positive heat of mixing ($\Delta H_{mix} = 0.5$ eV); it may even be due to the fact that the splining of the low-energy many-body potential to the high-energy ZBL potential becomes increasingly difficult with increasing ΔH_{mix}.

D. Mass effects

We also investigated the influence of the atomic mass on the mixing, leaving all potential parameters identical to those of Cu. To this end we bombarded a bilayer system, in which the first six layers consist of natural Cu, and the substrate of heavy (or light) Cu with twice (or half) the mass of natural Cu. The broadening in these systems is shown in Fig. 9(a), and compared to the deposited energy in these two systems. Obviously, the effect of mass is small; however, some systematic trends can be observed. In the light substrate, atom motion is definitely enhanced as compared to the heavy substrate. This correlates with a similar effect in the deposited energy distribution, Fig. 9(b), which may be due to the fact that heavy overlayer atoms have a higher chance of depositing energy in a light substrate than vice versa. In the overlayer, on the other hand, we observe that broadening—and the deposited energy—is increased if the substrate is heavy. This may stem from an increased backscattering of light overlayer atoms from the heavy substrate, which helps to confine the cascade in the overlayer. We conclude that the effect of mass on the broadening in bilayer systems appears to be correlated with or even based on its effect on the deposited energy distribution.

E. Effect of deposited energy

While the deposited energy is not a material parameter, we decided to include it into our study, since the various phenomenological models available predict quite a different dependence on this quantity.[5,13,14] It varies from linear for the mixing in so-called local spikes to quadratic in the mixing of a cylindrical spike, cf. Eq. (8).

We varied the deposited energy by changing the bombarding energy of the Cu projectile between 0.5 and 2 keV. As Fig. 10 displays, the broadening depends quadratically on the deposited energy. Deviations from this rule are only observed at the lowest bombarding energy,

where the effect of the cascade on the sixth and seventh layer is small. Such a quadratic dependence is, in fact, included in the phenomenological model given above, Eq. (8). Again the quantitative agreement of the model with our simulation is astonishingly good.

We note that in the energy regime studied by us the deposited energy increases linearly with the bombarding energy, cf. Fig. 10(b). Here, we defined the deposited energy as F_D, Eq. (3). Figure 11 shows the change of the deposited energy distribution with increasing bombarding energy. It is clearly seen how the maximum of the deposited energy shifts into the target inner with increasing bombarding energy and how the entire distribution broadens out. We note that for bombarding energies above about 2 keV, our simulation crystallite is too small to hold the entire cascade.

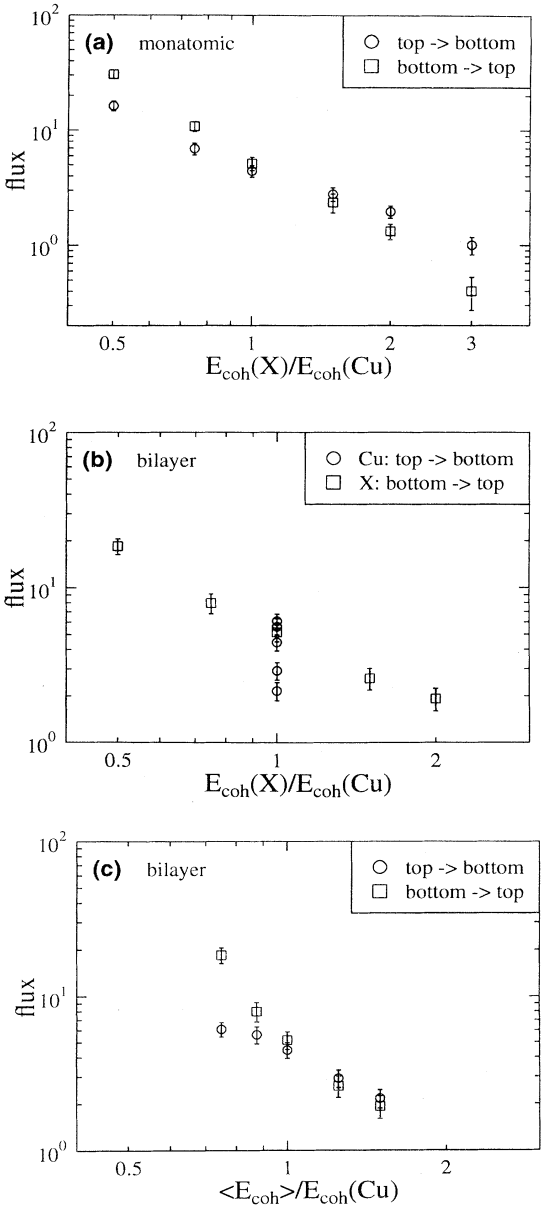

FIG. 6. Displaced particle fluxes through the interface between the sixth and seventh monolayers for elemental samples (a) and for bilayers (b,c). System and notation as in Fig. 5.

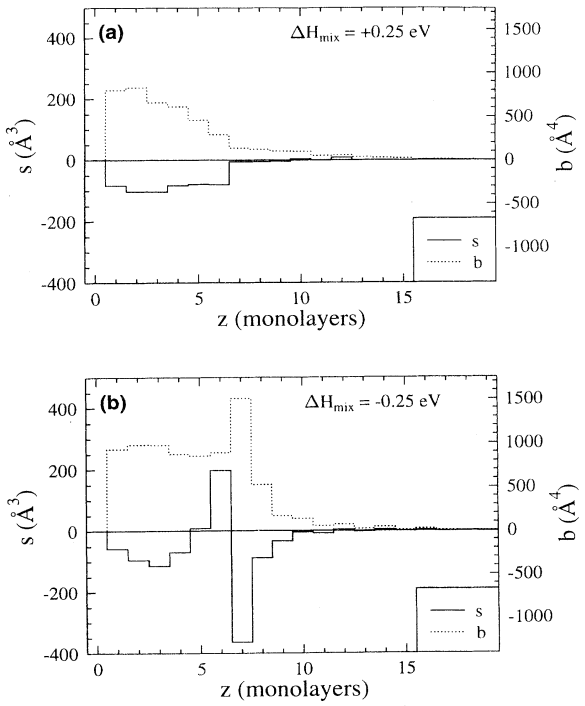

FIG. 7. Effect of the heat of mixing ΔH_{mix} on the broadening b and the shift s in a bilayer system in which the first six layers consist of natural Cu and the substrate of a modified Cu, which has a positive (a) or negative (b) heat of mixing towards Cu.

F. Random incidence

The simulations presented up to now were performed under perpendicular incidence, where the ion impinges in a normal (channeling) direction on a low indexed surface.

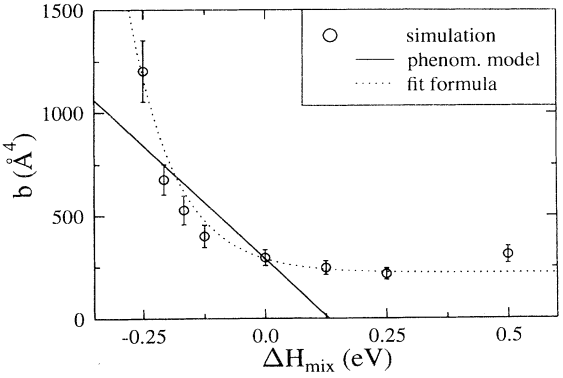

FIG. 8. Effect of heat of mixing ΔH_{mix} on the broadening b. Systems constructed as in Fig. 7. The solid line is the phenomenological model of Ref. 5, Eq. (8). The dotted line is the fit formula, Eq. (9).

It might be surmised that the results presented are atypical of the general situation of random incidence. In order to investigate this issue, we performed a simulation where elemental Cu with a (100) surface is bombarded in a nonchanneling direction. We chose an incidence angle of 10° towards the surface normal with random azimuth. The results are summarized in Fig. 12, where the shift, the broadening, and the deposited energy distribution for 10° incidence angle are presented and compared to the results for perpendicular incidence (Figs. 2 and 3). We observe only small differences. They stem mainly from the fact that the cascade appears to be more compact for random incidence: the tails of the deposited energy distribution and correspondingly of the broadening and the shift decay faster, and the corresponding values at smaller depths are slightly increased. However, the quantitative effect of nonrandom incidence is small. This is also evidenced by the sputter yield, which only changes from 5.2 to 6.3 when the bombarding angle is changed from 0° to 10°. It is evident that at other bombarding energies, the influence of the bombarding angle can be more important.

G. Other quantities

In Fig. 13, we display the dependence of the sputter yield on the cohesive energy for perpendicular incidence. It is seen that the yield increases more strongly than $1/E_{\mathrm{coh}}$, rather like $E_{\mathrm{coh}}^{-1.4}$. A roughly inverse dependence is predicted from analytical theory,[23] and has been shown by computer simulations previously,[27] where binary interaction potentials were used. A stronger increase of the yield with decreasing cohesive energy may be taken as a sign of a relatively small bombarding energy, where the asymptotic analytical theory does not yet hold; on the other hand, it might be an effect of the crystalline target structure. We also include in this figure the number of adatoms formed. It obeys a similar dependence. The ratio of the adatom to sputter yield is of the order of 3 to 4, as has been observed previously.[28] In Fig. 13(b), we show the number of surface and bulk vacancies produced per ion impact as a function of the cohesive energy of the material. We define as surface vacancies those which exist in the first monolayer. Obviously the number of vacancies formed increases with decreasing cohesive energy;

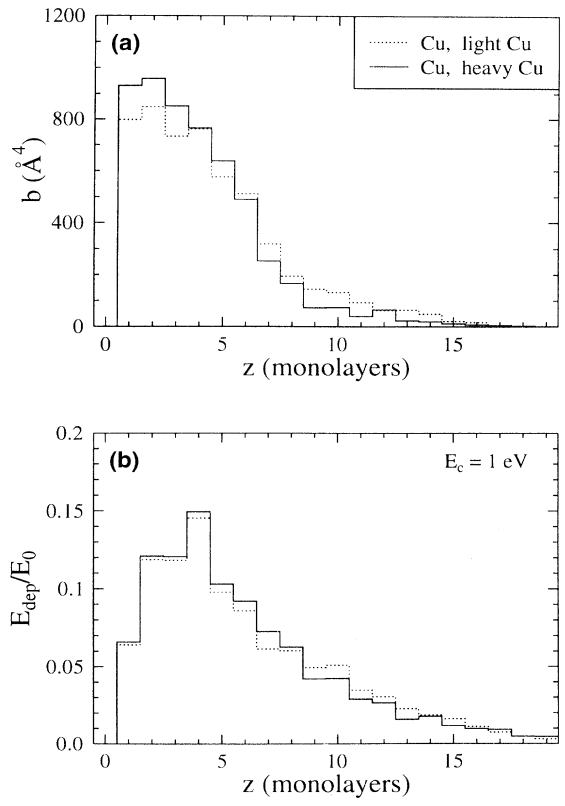

FIG. 9. Effect of atom mass on the broadening b and the shift s (a) and the energy deposited in recoil motion $E_{\mathrm{dep}}^{(2)}(z,E_c=1$ eV) (b), in a bilayer system consisting of six monolayers of natural Cu on top of a substrate of heavy (light) Cu with twice (half) the mass of natural Cu.

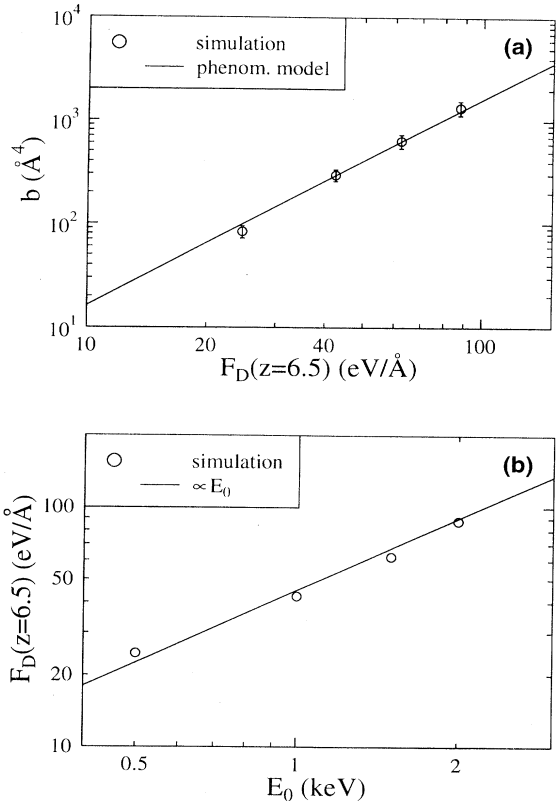

FIG. 10. (a) Effect of deposited energy F_D $(z=6.5)$ on the broadening b $(z=6.5)$ in layers 6 and 7 of a pure Cu metal. The line is the phenomenological model of Ref. 5, Eq. (8). (b) Dependence of the deposited energy F_D $(z=6.5)$ on the bombarding energy E_0. The line denotes proportionality of F_D with E_0.

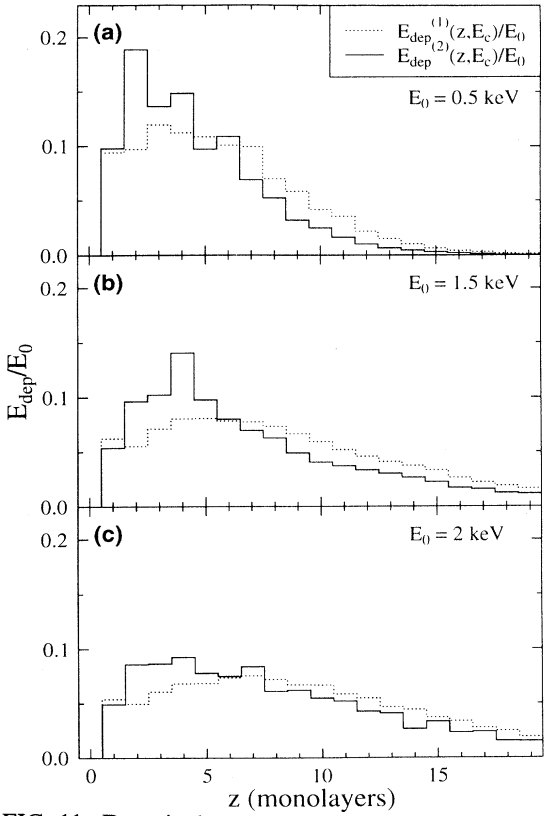

FIG. 11. Deposited energy distribution monitored according to two different detection schemes, cf. Fig. 2 and Eqs. (1) and (2), for various bombarding energies E_0 of a Cu projectile impinging on an elemental Cu target.

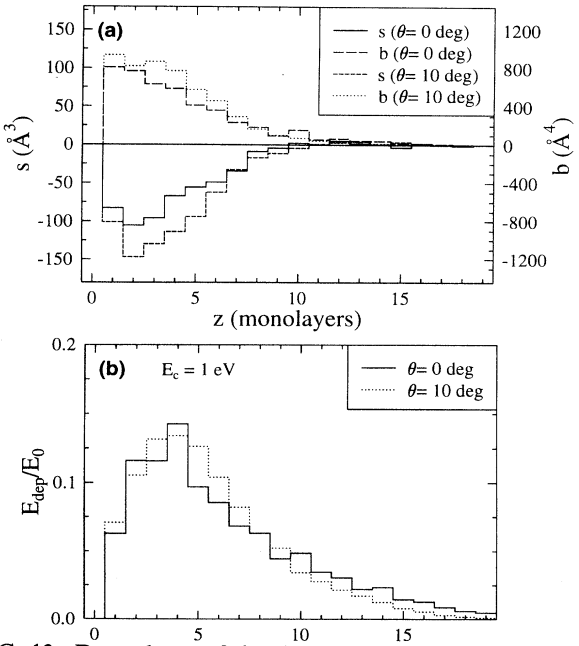

FIG. 12. Dependence of the shift s and the broadening b (a) and the energy deposited in recoil motion $E_{dep}^{(2)}(z,E_c=1\text{ eV})$ (b) on the bombarding angle θ. Results are shown for perpendicular incidence ($\theta=0°$), cf. Figs. 2 and 3, and for oblique incidence at an angle of $\theta=10°$, with respect to the surface normal and random azimuth.

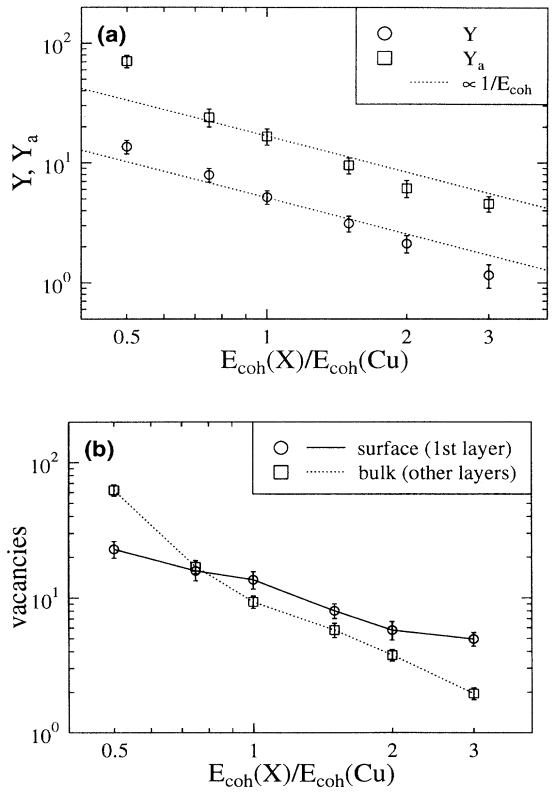

FIG. 13. (a) Sputtered atom yield Y and adatom yield Y_a, as a function of cohesive energy for elemental solids. Lines denote proportionality to $1/E_{coh}$. (b) Number of surface and bulk vacancies as a function of cohesive energy for elemental solids.

this is understandable, since we set the vacancy formation energy proportional to the cohesive energy, cf. Sec. II. The strong increase of the number of bulk vacancies for the smallest cohesive energy may be taken as an indication of strong crater formation under ion impact, which may occur under small cohesive energies; note that we do not distinguish between empty atoms sites in the crater and true bulk vacancies.

IV. SUMMARY

We presented a molecular-dynamics study on the effect of keV-ion bombardment on the mixing of metals. The study attempted to be systematic in the sense that the influence of two important materials parameters, viz. the heat of mixing and the cohesive energy, on the mixing was checked. Furthermore, we investigated the dependence of mixing on the deposited energy.

Focusing on the broadening as the decisive mixing characteristics, we found an inverse square dependence on the cohesive energy, and a stronger than linear dependence on the heat of mixing. Both features are in accordance with experimental data; the first dependence is a feature of many existing phenomenological models of mixing. Furthermore, we found a quadratic dependence on the deposited energy. Our simulation results can be

described astonishingly well by the phenomenological model of thermal spike mixing by Cheng *et al.*;[5,7] the agreement is quantitative with respect to the dependence on cohesive energy and deposited energy. Only the dependence on the heat of mixing as given by the phenomenological model is too crude.

For a reference case, the mixing of a pure Cu system, we also presented the spatial dependence of other quantities characteristic of mixing, such as the deposited energy distribution, the net number of particles displaced, and the mean displacement. Furthermore, a slightly stronger than inverse dependence of the sputter and the adatom yield on the cohesive energy was found, and the dependence of the number of surface and bulk vacancies on this quantity was investigated.

ACKNOWLEDGMENT

We acknowledge financial support by the Deutsche Forschungsgemeinschaft.

[1]G. Betz and G. K. Wehner, in *Sputtering by Particle Bombardment II,* edited by R. Behrisch (Springer, Berlin, 1983).

[2]H. H. Andersen, in *Ion Implantation and Beam Processing,* edited by J. S. Williams and J. M. Poate (Academic, Sydney, 1984), p. 127.

[3]*Materials Modification by High-Fluence Ion Beams,* Vol. 155 of *NATO Advanced Study Institute, Series E: Aplied Sciences,* edited by R. Kelly and M. F. da Silva (Kluwer, Dordrecht, 1989).

[4]H. Oechsner, *Thin Film and Depth Profile Analysis* (Springer, Berlin, 1984).

[5]Y.-T. Cheng, Mater. Sci. Rep. **5**, 45 (1990).

[6]A. Miotello and R. Kelly, Surf. Sci. **268**, 340 (1992).

[7]Y.-T. Cheng, M. Van Rossum, M.-A. Nicolet, and W. L. Johnson, Appl. Phys. Lett. **45**, 185 (1984).

[8]P. Sigmund and A. Gras-Marti, Nucl. Instrum. Methods **168**, 389 (1980).

[9]A. Gras-Marti and P. Sigmund, Nucl. Instrum. Methods **180**, 211 (1981).

[10]P. Sigmund and A. Gras-Marti, Nucl. Instrum. Methods **182/183**, 25 (1981); **195**, 639 (1982).

[11]W. Eckstein, *Computer Simulation of Ion-Solid Interactions* (Springer, Berlin, 1991).

[12]P. Sigmund, Appl. Phys. A **30**, 43 (1983).

[13]P. Børgesen, D. A. Lilienfeld, and H. H. Johnson, Appl. Phys. Lett. **57**, 1407 (1990).

[14]W. Bolse, Nucl. Instrum. Methods Phys. Res. Sect. B **80/81**, 137 (1993).

[15]T. Diaz de la Rubia, R. S. Averback, R. Benedek, and W. E. King, Phys. Rev. Lett. **59**, 1930 (1987).

[16]T. Diaz de la Rubia *et al.*, Nucl. Instrum. Methods Phys. Res. Sect. B **80/81**, 86 (1993).

[17]F. Karetta and H. M. Urbassek, J. Appl. Phys. **71**, 5410 (1992).

[18]H. Gades and H. M. Urbassek, Nucl. Instrum. Methods Phys. Res. Sect. B **69**, 232 (1992).

[19]H. Gades and H. M. Urbassek, Nucl. Instrum. Methods Phys. Res. Sect. B **88**, 218 (1994).

[20]R. W. G. Wyckoff, *Crystal Structures,* 2nd ed. (Wiley, New York, 1965).

[21]S. M. Foiles, M. I. Baskes, and M. S. Daw, Phys. Rev. B **33**, 7983 (1986).

[22]J. F. Ziegler, J. P. Biersack, and U. Littmark, *Stopping Powers and Ranges of Ions in Matter,* edited by J. F. Ziegler (Pergamon, New York, 1985), Vol. 1.

[23]P. Sigmund, in *Sputtering by Particle Bombardment I,* edited by R. Behrisch (Springer, Berlin, 1981), p. 9.

[24]H. M. Urbassek, G. Mayer, H. Gades, and M. Vicanek (unpublished).

[25]U. Conrad and H. M. Urbassek, Nucl. Instrum. Methods Phys. Res. Sect. B **83**, 125 (1993).

[26]P. Sigmund, A. Oliva, and G. Falcone, Nucl. Instrum. Methods Phys. Res. **194**, 541 (1982).

[27]D. E. Harrison, Jr., Radiat. Eff. **70**, 1 (1983).

[28]H. Gades and H. M. Urbassek, Phys. Rev. B **50**, 11 167 (1994).